Carbon scaffold structured silicon anodes for lithium-ion batteries

Juchen Guo, Xilin Chen and Chunsheng Wang*

Received 29th January 2010, Accepted 24th March 2010
First published as an Advance Article on the web 13th May 2010
DOI: 10.1039/c0jm00215a

A unique methodology of fabricating Si anodes for lithium-ion batteries with porous carbon scaffold structure is reported. Such carbon scaffold Si anodes are fabricated *via* carbonization of porous Si-PVdF precursors which are directly deposited on the current collector. Unlike the conventional slurry casting method, binder and conductive additives are not used in the preparation of the carbon scaffold Si anodes. The carbon scaffold Si anode has a close-knit porous carbon structure that can not only accommodate the Si volume change, but also facilitate the charge transfer reaction. These advantages are demonstrated by the superior capacity, cycle stability and rate performance of the carbon scaffold Si anodes.

Introduction

The lithium-ion battery has been recognized as the most promising energy storage technology for a wide range of applications, from consumer electronics, electric vehicles to renewable energy storage. Despite varying requirements of diverse applications, cost-efficient Li-ion batteries with high capacities and long cycling lives are generally essential. However, the low lithiation capacity (372 mA h g^{-1}) of the currently used graphite anodes has become one limiting factor in developing high-energy Li-ion batteries.[1]

Silicon is, potentially, an exceptional anode material due to its extraordinary lithiation capacity of 3579 mA h g^{-1} (the highest lithiation capacity at room temperature for chemical formula $Li_{15}Si_4$[2]). However, during Li insertion and extraction, Si undergoes volume expansion and shrinkage, which undermines the advantage of silicon's high capacity. Such a severe volume change (up to 270 vol%) can not only pulverize Si materials but also demolish the integrity of electrode structure, resulting in poor cycle stability.[3] For more than a decade, numerous investigations have been carried out to develop Si anodes with both high capacity and improved cycle stability. Among these efforts, Si-carbon composites have been demonstrated as the most successful category. Carbon is a good absorber for accommodating the Si volume change, and it is also electrically conductive, facilitating charge transfer reaction. A number of Si–carbon composite preparation techniques have been investigated. High-energy mechanical ball milling of a mixture of Si and carbon source material followed by pyrolysis is a well-studied method.[4–7] Preparation of carbon-coated Si particles through thermal or chemical vapor deposition (CVD) was also a popular method in early investigations.[8–11] Carbon-coated Si nanoparticles have been obtained *via* carbonization of carbon precursor-coated Si nanoparticles.[12–16] In addition to Si-carbon core–shell spherical structures, carbon–Si core–shell nanowires have also been obtained on carbon nanotubes by Si CVD,[17] and carbon-coated porous Si particles were obtained using silica templates.[18] Recently, carbon fibers with encapsulated Si nanoparticles were fabricated using the electrospinning technique.[19]

In contrast to those aforementioned techniques, the authors hereby report a unique methodology to fabricate Si anodes with a carbon porous scaffold structure. The concept of this scaffold anode (as illuminated by Fig. 1) is to incorporate the Si particles into a carbon scaffold with close-knit structure. The carbon scaffold has a vast amount of nanosized pores so that it can function as "absorber" to accommodate the strain and stress in the entire anode structure due to the Si volume change. In case of Si pulverization, the carbon scaffold structure with nanopores can hold the pulverized particles so avoiding Si exfoliation, which is superior to the electrospun C/Si composite nanofiber anodes[19] in which the pulverized Si could break off from electrodes through the micron-sized pores between nanofibers. Therefore, rather than preventing Si pulverization, the carbon scaffold reinforced Si anodes can sustain the overall electrode integrity in terms of microscopic structure and electrical connectivity between Si particles (even pulverized) and current collector. Moreover, the scaffold structure of Si anodes can facilitate the Li-ion transport and the charge transfer kinetics

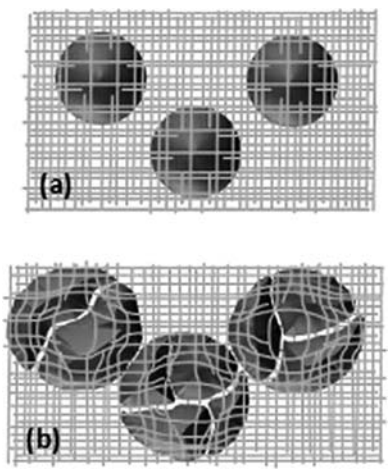

Fig. 1 Schematic of the structurally sustainable carbon scaffold Si anode (a) before lithiation, (b) after lithiation.

Department of Chemical & Biomolecular Engineering, University of Maryland, College Park, MD, 20742, USA. E-mail: cswang@umd.edu; Fax: +01 301-314-9126; Tel: +01 301-405-0352

thus improving the battery power. In this study, the carbon scaffold Si anode was obtained *via* carbonization of a Si-poly-(vinylidene fluoride) (PVdF) precursor scaffold which was directly deposited on a copper current collector using the slurry spray technique. The obtained 3D C/Si scaffold films were directly used as anodes for Li-ion batteries without adding any binder or conductive additive.

Experimental

Silicon nanoparticles (≥98%, average size 50 nm) were purchased from Sigma-Aldrich and used as received. Silicon micron-powder (325 mesh, particles size <44 μm) was also purchased from Sigma-Aldrich and was ball-milled for 24 h prior to electrode preparation. The Si-PVdF precursor was prepared using the slurry spray technique. (The detailed procedure has been discussed elsewhere.[20]) The slurry, consisting of 52 wt% Si particles, 12 wt% carbon black and 36 wt% PVdF (PVdF in 5 wt% *n*-methyl-2-pyrrolidone solution), was mixed for 1 h in an egg-shaped stainless steel vial using a Fritsch Pulverisette 6 mixer with zirconia balls as the milling media. The slurry was sprayed onto copper foil (current collector) at 140 °C using a Dayton Professional Air Brush Kit. Compressed nitrogen (40 psig) was used as the carrying gas, and the spray nozzle size of the air brush was about 0.10 mm in diameter. The distance between the nozzle and the current collector was kept constant at 18 cm. The obtained Si-PVdF scaffold precursor was carbonized at 700 °C in an argon-flowing tube furnace for 3 h with a heating ramp of 5 °C min^{-1}. The obtained carbon scaffold Si electrodes were then transferred to the argon-filled glove box for cell assembly.

Carbon-coated Si particles were also synthesized from carbonizing the same precursor (52 wt% of Si nanoparticles, 12 wt% of carbon black, and 36 wt% of PVdF) at 700 °C in an argon-flowing tube furnace for 3 h. The obtained powder was mixed with carbon black and PVdF (5 wt% in NMP solution) with 8 : 1 : 1 weight ratio in an egg-shaped stainless steel vial using a Fritsch Pulverisette 6 mixer with zirconia balls as the mixing media. The carbon-coated Si anodes were prepared by casting the slurry onto the copper foil, and then dried following the standard electrode preparation procedure. The electrochemical performance of anodes made of carbon-coated Si particles was compared to that of the carbon scaffold Si anodes.

Two-electrode coin cells with lithium foil as the counter electrode were used. Electrolyte consisting of 1 M $LiPF_6$ in a mixture of ethylene carbonate–diethyl carbonate (EC–DEC 1 : 1 by volume) was used with a microporous membrane separator (Celgard®3501). The cells were charged and discharged at different cycling currents between 0 and 1.5 V (*vs.* Li/Li^+) using an Arbin™ battery test station.

Scanning electron microscopy (SEM) images were taken using a Hitachi SU-70 Analytical Ultra-high Resolution scanning electron microscope. X-Ray diffraction (XRD) patterns were recorded on a Bruker Smart1000 using Cu-Kα radiation. The Raman spectrum was recorded on a Horiba Jobin-Yvon Lab-RAM microRaman system with 532 nm laser source. Thermogravimetric analysis (TGA) was carried out using a thermogravimetric analyzer (TA instruments) with a heating rate of 5 °C min^{-1} in air.

Results and discussion

Fig. 2 shows the XRD pattern of the obtained Si-carbon scaffold anode. Comparing the XRD pattern of the Si-carbon scaffold to the XRD pattern of the pure Si nanoparticles, the peaks indexed to crystalline Si can be identified. No detectable crystalline SiO_x phase was observed in the XRD pattern. A small iron peak can be attributed to a residue from the steel vial in which the slurry was prepared, as described in the Experimental section. The degree of graphitization of the carbon scaffold can be estimated from the characteristic wide D and G bands around 1350 and 1600 cm^{-1} in the Raman spectrum (Fig. 3). The peak centered near 1350 cm^{-1} (D band) can be explained as structure defect- and disorder-induced features in the graphene layers of carbon materials, while the peak centered near 1600 cm^{-1} (G band) is indicative of the high-frequency E_{2g} first-order graphitic crystallites of the carbon.[21–23] The presence of the strong D band suggests that the carbon component in these carbon scaffold Si anodes has low crystallinity and graphitization and is typical of disordered graphitic material. TGA was performed on the carbon scaffold Si anode in an air environment, and the result is shown in Fig. 4. The carbon scaffold Si anode retained 76 wt% after reaching 700 °C. Although it is considered that a thin layer of SiO_x could be formed during the TGA test, the carbon content

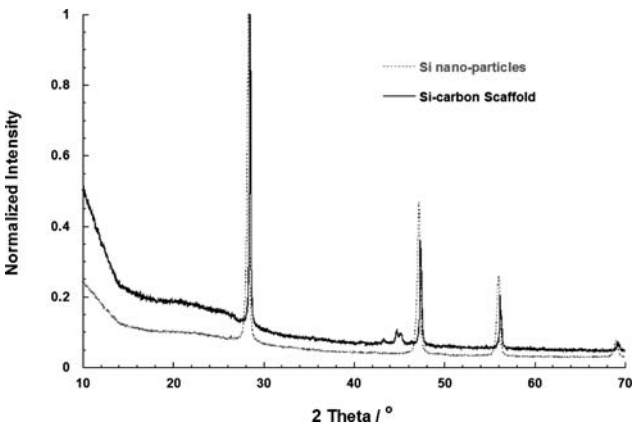

Fig. 2 XRD patterns of the pristine Si nanoparticles and the carbon scaffold Si anode.

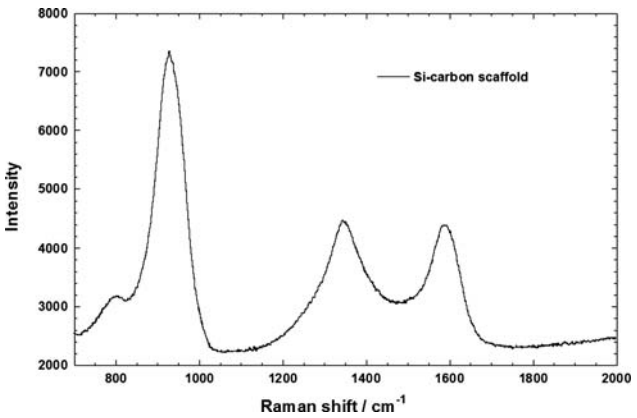

Fig. 3 Raman spectrum of the carbon scaffold Si anode.

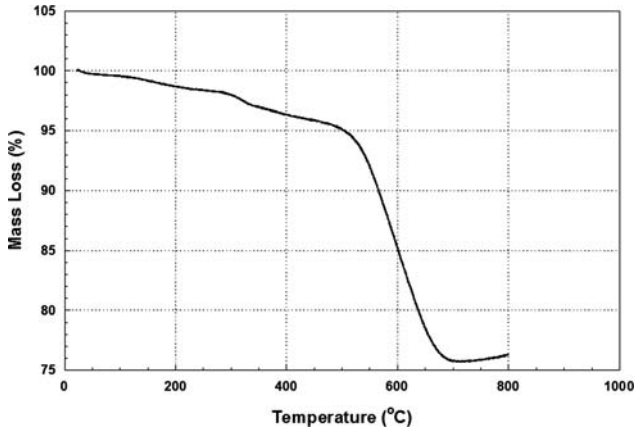

Fig. 4 TGA curve of the carbon scaffold Si anode in air.

Table 1 Surface area and porosity properties of the Si-PVdF precursor and the carbon scaffold Si anode

Sample	S_A/m^2 g^{-1}	d_p/nm	V_p/cm^3 g^{-1}
Si-PVdF Precursor	10.41	32.7	0.085
Si-Carbon scaffold	53.84	13.2	0.178

in the carbon scaffold Si anode can thus be estimated as 24 wt%.[14]

Nitrogen adsorption measurements (Brunauer–Emmett–Teller method) were performed on the Si-PVdF precursor and the Si-carbon scaffold anodes to obtain their specific surface area (S_A), pore volume (V_p) and average pore size (d_p) which are listed in Table 1. Nitrogen absorption isotherms and the accumulated pore volume *vs.* pore size of the Si-carbon scaffold are plotted in Fig. 5. A total specific pore volume of 0.085 cm^3 g^{-1} with average size of 32.7 nm was generated in the Si-PVdF precursor using the slurry spray technique. A large increase of total pore volume in the carbon scaffold Si anode was achieved during carbonization, resulting in a five-fold higher surface area than that in the Si-PVdF precursor and much smaller average pore size. The increase of surface area and total pore volume is believed to be a result of the partial decomposition of PVdF. The SEM images (Fig. 6) of the surface of Si-PVdF precursor and the surface of the resulting Si-carbon scaffold anode provide direct observations of the porous structures. It is immediately apparent that the carbon scaffold Si anode (Fig. 6b) is more porous than its precursor (Fig. 6a). The Si particles are bound within the carbon matrix, which is able to accommodate the Si volume change during charge/discharge cycles due to both the intrinsic softness of carbon and the porous structure. The excellent integrity of the Si-carbon scaffold in charge/discharge cycles has been directly evidenced from the SEM images of the carbon scaffold Si anode before (Fig. 6b) and after 142 full charge/discharge cycles between 0 and 1.5 V using 0.1C cycling rate (Fig. 6c). (The notation *n*C cycling rate means charging or discharging an electrode at full capacity in 1/*n* hours. In this study, full capacity of Si is taken as 2000 mA h g^{-1}. Therefore, 0.1C cycling rate is equivalent to 200 mA g^{-1} cycling current density.) From Fig. 6c, it can be seen that the porous structure of the Si-carbon scaffold

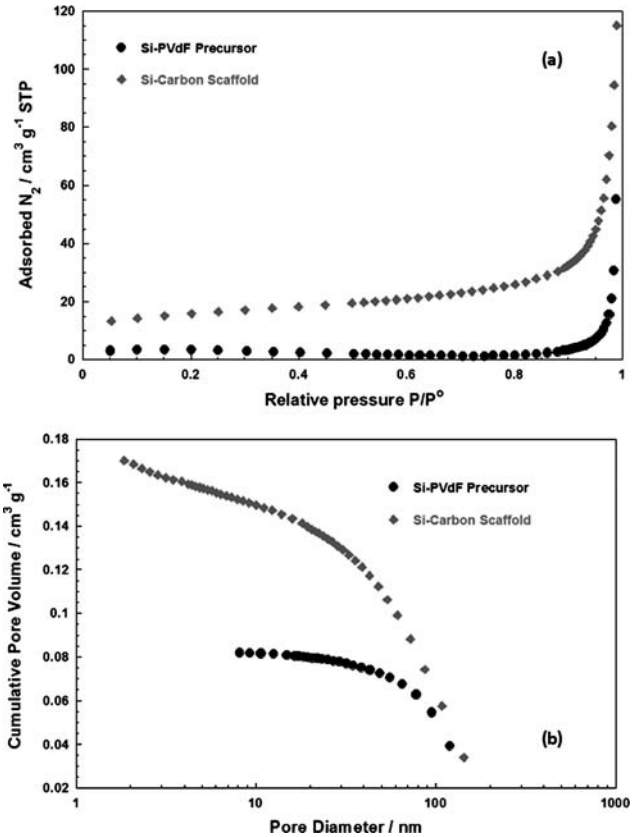

Fig. 5 (a) N_2 adsorption isotherms of Si-carbon scaffold and (b) Si-carbon scaffold cumulative pore volume *vs.* the pore diameter.

is well retained even after intensive cycling. The solid electrolyte interface (SEI) film can be identified on the surface of the Si-carbon scaffold based on the slightly thickened structure. However, the surface was not entirely covered, which suggests a stable SEI film. This observation could be speculated as an advantage of the carbon scaffold. A recently study by Yen *et al.*[24] suggested that a carbon coating on Si could help to stabilize the formation of the SEI film. This observation of Fig. 3c agrees with this conclusion.

The electrochemical performance of the obtained carbon scaffold Si anodes are shown in Fig. 7. Fig. 7a shows the charge (Li extraction) capacity retention and the coulombic efficiency (ratio of charge capacity to discharge capacity in each cycle) under three different cycling rates, 0.05C, 0.1C and 0.2C from 0 to 1.5 V. The carbon scaffold anode could retain 1792 mA h g^{-1} capacity (81.3% retention) after 123 full cycles under 0.05C. The usable charge capacity was 1337 mA h g^{-1} (60.9% retention) after 142 full cycles under 0.1C and 1403 mA h g^{-1} (68.8% retention) after 112 full cycles under 0.2C, respectively. The irreversible capacity in the first charge/discharge cycle under 0.05C, 0.1C and 0.2C were 34.6%, 31.6% and 32.8%, respectively. The coulombic efficiency quickly increased to about 95% at the second cycle, and then reaching 99.9% after at most five cycles.

Fig. 7b shows the charge rate capacities of the carbon scaffold Si anode under various charge rates. All anodes were discharged (Li insertion) using the 0.05C rate (100 mA g^{-1}), and charged (Li extraction) at varying rates. A total of 75 full cycles, with at least 11 cycles under each charge rate, were tested. The Si-carbon

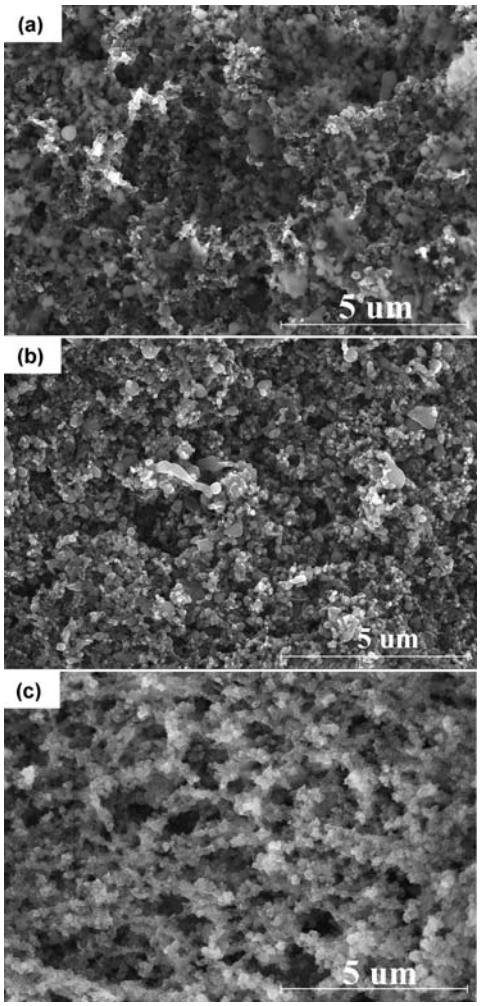

Fig. 6 SEM images of (a) Si-PVdF precursor, (b) Si-carbon scaffold anode and (c) Si-carbon scaffold anode after 142 cycles between 0 and 1.5 V with 200 mA g^{-1} charge/discharge current density.

scaffold anode was demonstrated to have exceptionally high rate capability. It could retain 1379 mA h g^{-1} capacity at 1.5 C rate (3 A g^{-1} charge current density). This excellent rate capacity performance indicates that the porous structure of carbon scaffold Si anodes not only can accommodate the Si volume change but also can facilitate Li-ion transport in the anode and the charge transfer kinetics because of the increased reaction area.

The carbon scaffold structure can not only be used for nano-Si particles, but also is feasible for micron-sized Si powder. Fig. 8 shows the cycle stability results of the carbon scaffold anodes with micron-Si particles with particle size of about 2 μm. The carbon scaffold micron-Si anode could retain 1280 mA h g^{-1} capacity after 118 full cycles between 0 and 1.5 V under 0.05C cycling rate. The usable charge capacity was 960 mA h g^{-1} after 105 full cycles under 0.1C and 680 mA h g^{-1} after 107 full cycles under 0.2C, respectively. The irreversible capacity in the first charge/discharge cycle under 0.05C, 0.1C and 0.2C were 33.1%, 35.0% and 29.6%, respectively. The coulombic efficiency quickly increased to above 99.0% after a few cycles. These cycling stability results of unoptimized micron-Si anodes under 0.0–1.5 V (100% depth of charge/discharge) cycles are even

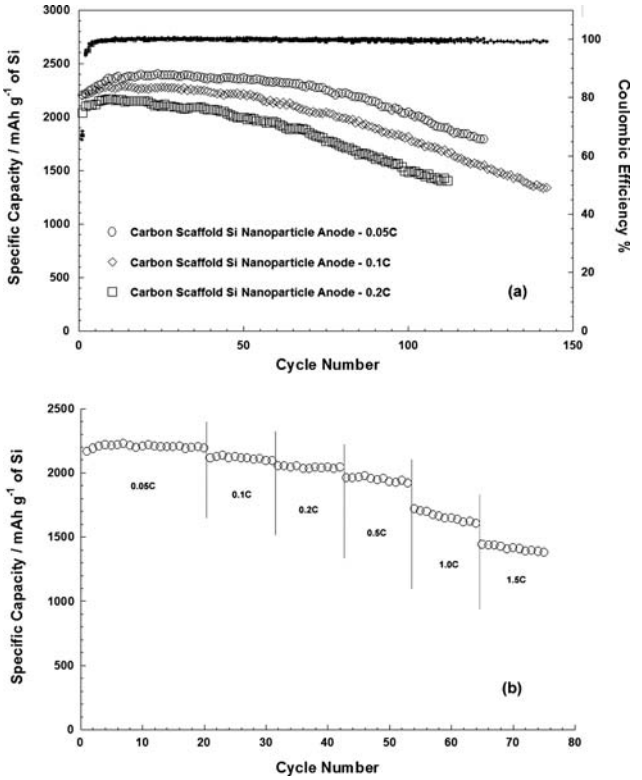

Fig. 7 (a) Delithiation capacity retention and cycle stability tests of carbon scaffold anodes made of Si nanoparticles at 0.05C (circles), 0.1C (diamonds), and 0.2C (squares); (b) delithiation capacity performances at various cycling rates.

comparable to the capacity retention of traditional micron-Si anodes cycled in a shallow potential window of 0.17– 0.9 V to avoid the most severe Si volume change through sacrificing the capacity.[25] Instead, we cycled the cells without lower cutoff voltage limit. Therefore the micron-Si anode results shown here represent the worst case of charge/discharge scenario.

The carbon scaffold Si anode also demonstrated better electrochemical performance than the CMC scaffold Si anode,[20] especially for the micron-sized Si particles. The capacity retention improved from 930 mA h g^{-1} after 85 cycles (CMC) to

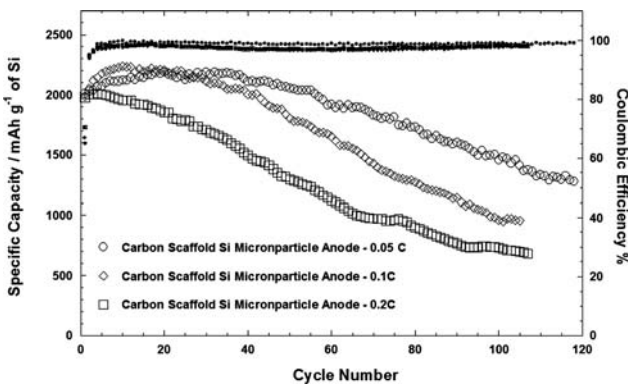

Fig. 8 Delithiation capacity retention and cycle stability tests of carbon scaffold anodes made of Si micron particles at 0.05C (circles), 0.1C (diamonds) and 0.2C (squares).

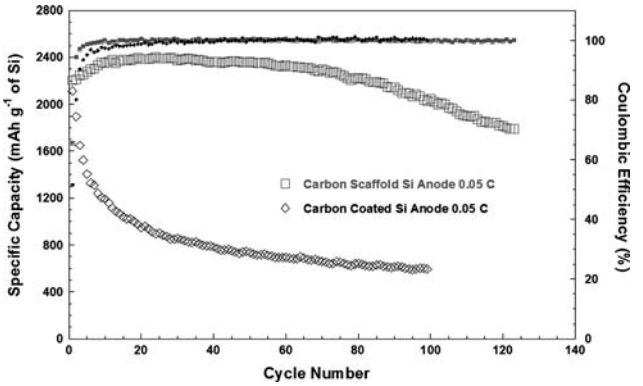

Fig. 9 Cycling stability of the carbon scaffold Si anode (squares) and carbon-coated Si anode (diamonds).

1280 mA h g^{-1} after 118 cycles (carbon). The rate capacity performance of the Si/carbon anode is also better than that of the Si/CMC one because of the higher electrical conductivity of carbon than that of CMC.

This carbon scaffold Si anode presented here is different from the C/Si anodes made from carbon-coated Si particles (through pyrolysis of PVDF[15]), binder and carbon black using the conventional slurry coating method. Fig. 9 shows cycling behaviors of the Si-carbon scaffold anode and the carbon-coated Si anode. The composition and synthesis procedure of the C/Si material in both anodes are the same. The only difference is the electrode structure: the carbon scaffold Si anode is formed by carbonization a Si/PVdF precursor directly deposited on the current collector by a slurry spray, while traditional carbon-coated Si electrodes are fabricated using a slurry casting method with PVdF binder and carbon black. As shown in Fig. 9, the carbon scaffold greatly enhanced charge/discharge cycling stability of the Si anode. The initial capacity of carbon-coated Si anode was similar to that of the carbon scaffold Si anode, but it decreased distinctly faster, which is consistent with the results reported by Liu *et al.*[15] It suggested that the integrity of the carbon scaffold structure was the main reason for the superior performance of the carbon scaffold Si anode.

To understand the mechanism of the capacity fading after intensive cycling, the electrochemical resistance of the carbon scaffold Si nanoparticle anode was measured using electrochemical impedance spectroscopy (EIS). The EIS measurements were carried out over a frequency range from 1000 kHz to 1 mHz with an ac amplitude of 10 mV on a Solartron™ SI1287/1260 analyzer. EIS measurements were performed after the 1st, 2nd, 3rd, 20th, 45th, 55th, 75th and 110th cycles (anode fully lithiated) under the 0.1C cycling rate. The Nyquist plots of these EIS measurements are plotted in Fig. 10. The internal impedance of the cell can be described by its equivalent circuit, which is plotted as the inset of Fig. 10a. In the equivalent circuit, R_s is the resistance associated with the cell components, such as the electrolyte, the working electrode (carbon scaffold Si anode) and the counter electrode (Li foil). R_{int} is the interface resistance relevant to the SEI film, R_{ct} is the charge-transfer resistance for the electrode reaction, and W is the Warburg contribution that is related to Li-ion diffusion into the Si-carbon scaffold. Because of the porous structure of the carbon scaffold Si anode, the capacitor

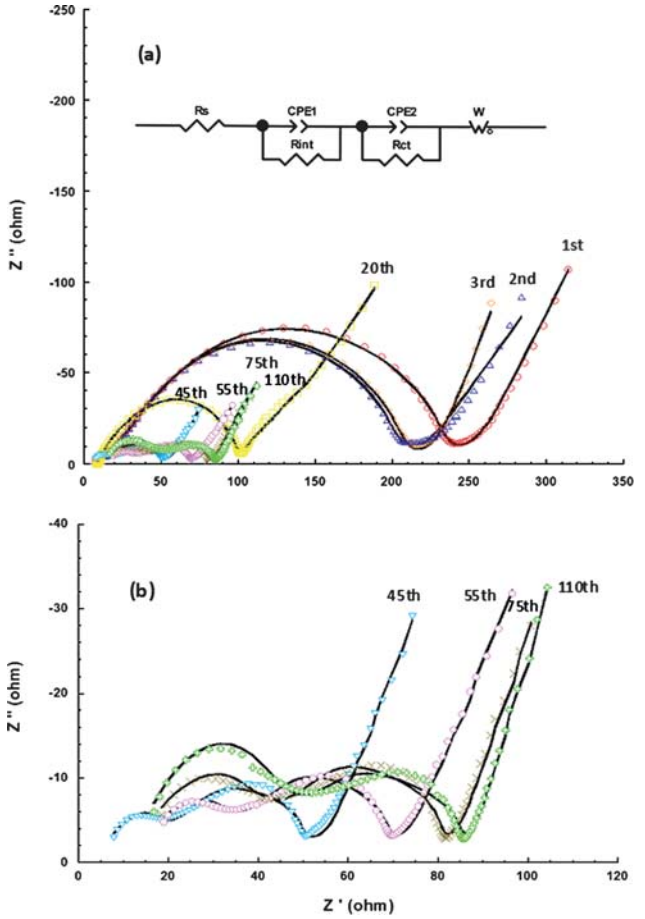

Fig. 10 (a) Nyquist plots of carbon scaffold Si nanoparticle anode after a series of cycles under 0.1C; (b) close-up of Nyquist plots for the 45th, 55th, 75th and 110th cycles. The symbols represent the EIS measurement data, and the lines are fitting curves using the equivalent circuit.

component in the equivalent circuit was replaced by the constant phase element (CPE).[26] The obtained impedances can be well fitted with the equivalent circuit. The total impedance decreased initially, and then began to slowly increase after the 45th cycle. The improved reaction kinetics during the initial 45 charge/discharge cycles resulted in an initial capacity increase and stabilization observed in Fig. 7a (activation process). Although the electrode impedance slowly increased after the 45th charge/discharge cycles, the impedance in the Si/carbon scaffold anode at the 110th cycle is still less than that in early cycles. Therefore, the continuous capacity fade at high number of cycles can not be attributed to the worsened kinetics. Instead, the possible reason can be the continuous disconnection of active Si materials over the repeated cycling. Therefore, it indicates that the mechanical durability of the carbon scaffold is of great importance to the carbon scaffold Si anode.

Conclusions

The carbon scaffold Si anode was obtained *via* carbonization of a Si-poly(vinylidene fluoride) (PVdF) precursor scaffold which was directly deposited on a copper current collector using the slurry spray technique. The obtained 3D C/Si scaffold films were

directly used as anodes for Li-ion batteries without adding any binder or conductive additive. This carbon scaffold Si anode showed superior cycling stability over the carbon-coated Si anode using a conventional slurry coating method. The exceptional cycling stability and rate capability of carbon scaffold structured Si anodes is attributed to the unique close-knit carbon scaffold structure in which the vast number of nanosized pores can (1) accommodate the volume change of Si thus retaining the integrity of the electrode, and (2) facilitate the Li-ion transport and the charge transfer kinetics. The promising performance of the carbon scaffold anodes with micron-sized Si particles demonstrates the potential feasibility of transforming this technique to commercialization. The future work will focus on Si/carbon scaffold anodes with a well patterned 3D structure, optimum pore size, pore distribution, and improved integrity.

References

1 M. Yoshio, T. Tsumura and N. Dimov, *J. Power Sources*, 2005, **146**, 10–14.
2 M. N. Obrovac and L. Christensen, *Electrochem. Solid-State Lett.*, 2004, **7**, A93–A96.
3 A. Magasinski, P. Dixon, B. Hertzberg, A. Kvit, J. Ayala and G. Yushin, *Nat. Mater.*, 2010, **9**, 353, DOI: 10.1038/nmat2725.
4 C. S. Wang, G. T. Wu, X. B. Zhang, Z. F. Qi and W. Z. Li, *J. Electrochem. Soc.*, 1998, **145**, 2751–2758.
5 D. Larcher, C. Mudalige, A. E. George, V. Porter, M. Gharghouri and J. R. Dahn, *Solid State Ionics*, 1999, **122**, 71–83.
6 Y. Liu, K. Hanai, J. Yang, N. Imanishi, A. Hirano and Y. Takeda, *Electrochem. Solid-State Lett.*, 2004, **7**, A369–A372.
7 X.-W. Zhang, P. K. Patil, C. Wang, A. J. Appleby, F. E. Little and D. L. Cocke, *J. Power Sources*, 2004, **125**, 206–213.
8 M. Yoshio, H. Wang, K. Fukuda, T. Umeno, N. Dimov and Z. Ogumib, *J. Electrochem. Soc.*, 2002, **149**, A1598–A1603.
9 N. Dimov, K. Fukuda, T. Umeno, S. Kugino and M. Yoshio, *J. Power Sources*, 2003, **114**, 88–95.
10 W.-R. Liu, J.-H. Wang, H.-C. Wu, D.-T. Shieh, M.-H. Yang and N.-L. Wua, *J. Electrochem. Soc.*, 2005, **152**, A1719–A1725.
11 M. Holzapfel, H. Buqa, F. Krumeich, P. Novák, F.-M. Petrat and C. Veit, *Electrochem. Solid-State Lett.*, 2005, **8**, A516–A520.
12 S.-H. Ng, J. Wang, D. Wexler, K. Konstantinov, Z.-P. Guo and H.-K. Liu, *Angew. Chem., Int. Ed.*, 2006, **45**, 6896–6899.
13 R. D. Cakan, M.-M. Titirici, M. Antonietti, G. Cui, J. Maier and Y.-S. Hu, *Chem. Commun.*, 2008, 3759–3761.
14 Y.-S. Hu, R. Demir-Cakan, M.-M. Titirici, J.-O. Muller, R. Schlogl, M. Antonietti and J. Maier, *Angew. Chem., Int. Ed.*, 2008, **47**, 1645–1649.
15 Y. Liu, Z. Y. Wen, X. Y. Wang, A. Hirano, N. Imanishi and Y. Takeda, *J. Power Sources*, 2009, **189**, 733–737.
16 Q. Si, K. Hanai, N. Imanishi, M. Kubo, A. Hirano, Y. Takeda and O. Yamamoto, *J. Power Sources*, 2009, **189**, 761–765.
17 Li-F. Cui, Y. Yang, C.-M. Hsu and Y. Cui, *Nano Lett.*, 2009, **9**, 3370–3374.
18 H. Kim, B. Han, J. Choo and J. Cho, *Angew. Chem., Int. Ed.*, 2008, **47**, 1–5.
19 L. Ji and X. Zhang, *Electrochem. Commun.*, 2009, **11**, 1146–1149.
20 J. Guo and C. Wang, *Chem. Commun.*, 2010, **46**, 1428–1430.
21 C. Kim, S. Park, J. Cho, D. Lee, T. Park and W. Lee, *J. Raman Spectrosc.*, 2004, **35**, 928–933.
22 C. Kim, Y. I. Jeong, B. T. N. Ngoc, K. S. Yang, M. Kojima and Y. A. Kim, *Small*, 2007, **3**, 91–95.
23 J. T. McCann, B. Lim, R. Ostermann, M. Rycenga, M. Marquez and Y. Xia, *Nano Lett.*, 2007, **7**, 2470–2474.
24 Y.-C. Yen, S.-C. Chao, H.-C. Wu and N.-L. Wua, *J. Electrochem. Soc.*, 2009, **156**, A95–A102.
25 M. N. Obrovac and L. J. Krause, *J. Electrochem. Soc.*, 2007, **154**, A103–A108.
26 D. Aurbach, M. D. Levi, E. Levi, H. Teller, B. Markovsky and G. Salitra, *J. Electrochem. Soc.*, 1998, **145**, 3024–3034.

